

镁/钢异种材料点焊接头力学性能及显微组织分析

陈益平, 邵景辉, 胡德安, 程东海

(南昌航空大学 材料学院, 南昌 330063)

摘 要: 采用三相次级整流电阻焊机进行镁/钢异种材料电阻点焊, 研究并确定了工艺参数范围和最佳数值。通过金相显微镜观察了接头的显微组织特征, 并采用显微硬度计测试了接头各区域的显微硬度。结果表明, 接头的剪切力随着焊接时间(2~14周波)、焊接电流(20~37.5 kA)以及电极力(5~8 kN)的增大均呈先增大后减小的趋势。当焊接时间8周波、焊接电流32 kA、电极力7 kN时, 最大接头剪切力达6.961 kN, 形成纽扣断裂。接头由半椭圆形镁合金熔核和钢侧热影响区组成, 镁侧熔核显微组织由柱状晶和等轴晶组成, 钢侧热影响区显微组织为板条状马氏体。镁侧离熔合线越近硬度越高, 而钢侧最高硬度出现在钢板的中心。

关键词: 异种材料; 电阻点焊; 工艺参数; 显微组织

中图分类号: TG115.28 **文献标识码:** A **文章编号:** 0253-360X(2013)04-0101-04



陈益平

0 序 言

汽车轻量化已成为当今汽车工业发展的必然趋势。在汽车制造中增加高强度钢、镁合金等轻量化材料的使用是实现汽车轻量化的最有效的方法之一^[1]。镁合金是目前实际应用中最轻的金属合金化结构材料, 被誉为21世纪重要的商用轻质材料^[2,3]。目前正在使用和研制的镁合金汽车零部件有60多种, 在未来汽车工业的发展过程中, 镁合金用量将大幅度增加。随着镁合金在汽车上应用的增多, 随之而来的镁/钢异种材料的焊接便成为亟待解决的问题。

由于镁/钢两种材料在性能上有很大的差异, 且其晶格类型也不同, 镁是密排六方结构, 钢在熔融态是体心立方结构, 从而造成它们在液态下极难互溶^[4], 因此采用传统的熔焊焊接方法进行焊接时, 很难形成焊缝。目前关于镁/钢焊接的研究很少, 目前主要涉及的焊接方法有激光-电弧复合热源焊、激光深熔钎焊以及搅拌摩擦焊。然而, 由于在焊接过程中出现MgO、ZnO、Fe₂O₃和Al₂O₃等金属氧化物, 以至于得不到强度高的焊接接头。且这些方法效率低, 难以满足大批量生产的需求。主要用于薄壁件产品生产的电阻点焊技术以其高效、可靠的连接在工业界已经获得广泛青睐^[4]。因此如果能用电

阻点焊的方法得到强度更高的焊接接头, 这将极大的促进镁/钢焊接接头的实际应用。而且目前几乎没有关于镁/钢异种材料电阻点焊的报道, 至今还没有镁合金与镀锌钢板电阻焊的报道。文中通过试验研究镁/钢异种材料点焊工艺参数对接头力学性能以及组织的影响, 从而确定合理的工艺参数, 为实际生产应用提供一些理论依据。

1 试验方法

试验选用2 mm厚的AZ31B镁合金以及1 mm的SPHC镀锌钢板材作为电阻点焊的焊接材料, 化学成分含量如表1、表2所示。

表1 AZ31B镁合金化学成分含量(质量分数, %)

Table 1 Chemical compositions of AZ31B magnesium alloy

Si	Zn	Mn	Al	Fe	Cu	Mg
0.025	0.96	0.32	3.18	0.002 2	0.003 5	余量

表2 SPHC镀锌钢化学成分含量(质量分数, %)

Table 2 Chemical compositions of SPHC galvanized steel

C	Si	Mn	P	S	Al
≤0.12	≤0.05	≤0.50	≤0.035	≤0.035	≥0.010

采用KDWJ-17型三相次级整流电阻焊机进行焊接试验, 电极材料选用铬锆铜合金(CuCrZr), 镁

合金侧用端面直径为 20 mm 的球面电极,其球面半径为 150 mm,镀锌钢板侧用端面直径为 25 mm 的平面电极,将试样加工成尺寸为 100 mm × 25 mm,长度方向上搭接为 20 mm,如图 1 所示。

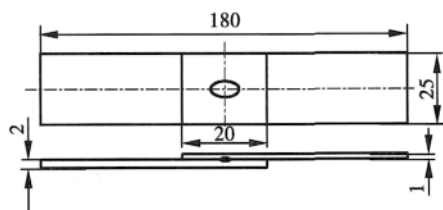


图 1 焊件试样示意图 (mm)

Fig. 1 Schematic diagram of weldment

试验采用 WDW4504 型微机控制电子万能试验机对不同参数下的试样进行拉伸试验,其拉伸速度为 1 mm/min。焊后沿焊缝横截面切取试样并制备成金相试样,经 3% 硝酸酒精溶液腐蚀 (2 ~ 4 s) 后,采用金相显微镜进行观察和分析。显微硬度测试在 HVS-1000 型显微硬度仪上进行,试样放大倍数 400 倍,试验采用的加载持续时间为 10 s,加载重量为镁侧 1 N,钢侧 2 N。

2 试验结果及分析

2.1 工艺参数对接头力学性能的影响

2.1.1 焊接电流

在电极力和焊接时间分别为 7 kN 和 8 周波的条件下,研究焊接电流 (20 ~ 37.5 kA) 的影响规律。结果表明,随着电流从 20 kA 上升到 32.5 kA,接头拉剪力从 2.536 kN 增加到 6.961 kN。当焊接电流小于 20 kA 时,无法形成熔核,而当焊接电流大于 32.5 kA 时,由于加热过于强烈会产生后期飞溅,从而导致剪切力的减小。在实际生产中应避免出现飞溅的点焊接头,为了提高接头的力学性能,选择 20 ~ 32 kA 的工艺参数较为适宜。

2.1.2 电极力

在电极电流和焊接时间分别为 32 kA 和 8 周波的条件下,研究电极力 (5 ~ 8 kN) 对接头力学性能的影响规律。当电极力从 5 kN 增加到 8 kN 时,接头的剪切力先是逐渐增大,到达最高点后又逐渐减小,当电极力为 7 kN 时,剪切力达到最大值 6.961 kN。当电极力过小时 (小于 5 kN),会导致总电阻的增大,热输入量过多而散热较差,焊接区的金属塑性变形程度不够,造成因电流密度过大而引起的加热速度大于塑性环扩张的速度,从而引起较大的飞溅,

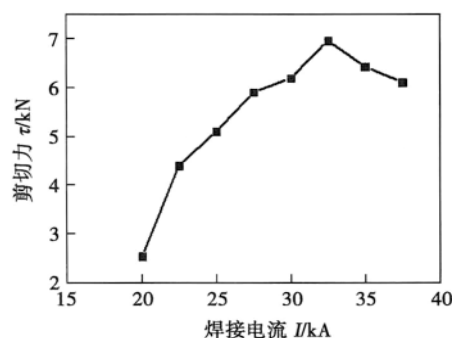


图 2 焊接电流对剪切力的影响

Fig. 2 Effects of welding current on joint tensile shear load

最后影响了接头的强度。当电极力过大时 (大于 8 kN), 因为电极散热量过大, 热输入不足而形成熔核过小, 因此选择电极力范围为 5 ~ 8 kN。

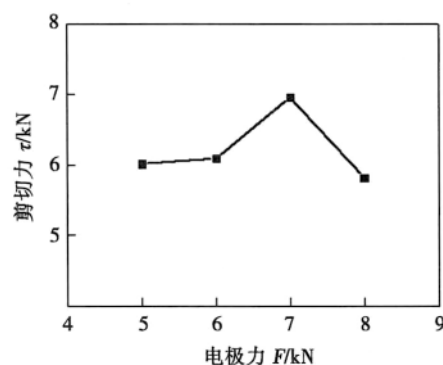


图 3 电极力对剪切力的影响

Fig. 3 Effects of electrode force on joint tensile shear load

2.1.3 焊接时间

对焊接时间 (2 ~ 14 周波) 的影响研究是在焊接电流和电极力分别为 32 kA 和 7 kN 的条件下进行的。图 4 为焊接时间对接头剪切力的影响。当焊接时间从 2 ~ 8 周波时,接头的剪切力明显提高,从 3.758 kN 增加到 6.961 kN,而 8 个周波以后,接头的剪切力反而有所下降,主要是因为焊接时间过长导致组织粗化、接头形成裂纹。因此选择焊接时间范围是 6 ~ 10 周波。在试验参数范围内,最佳工艺为 $t=8$ 周波 $I=32$ kA $F=7$ kN。

2.2 接头的显微组织分析

图 5 为接头的截面整体形貌,图 5 中 A ~ D 分别为点焊接头凝固过程中所处不同区域的各点。

图 6 为相对应的接头各区域显微组织形貌。图 6a 为接头热影响区域,它介于熔核和母材之间,为母材和熔核的过度区域,此区域为一层厚度不一的较窄区域围绕在熔核周围呈环状分布,相比母材

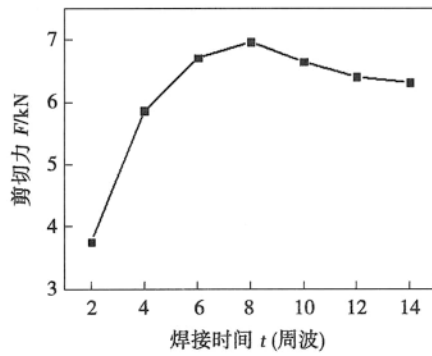


图4 焊接时间对剪切力的影响

Fig. 4 Effects of welding time on joint tensile shear load

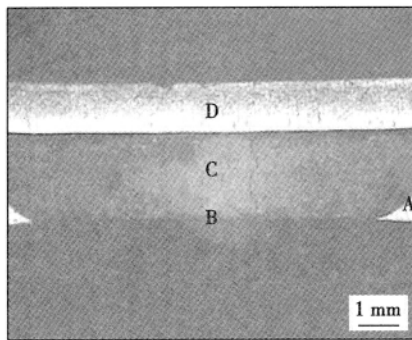
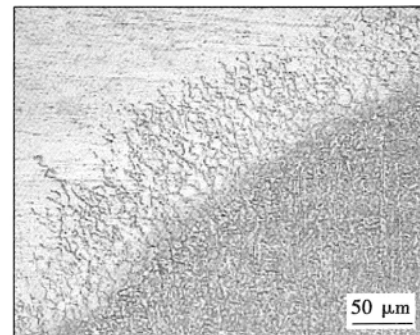


图5 接头的截面形貌

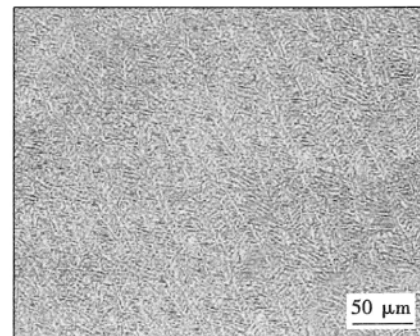
Fig. 5 Sections of spot welding joints

和熔核区域的晶粒,其晶粒明显粗大,且大小不一,分布不均.半固态的热影响区晶粒的晶界及晶内不断地连续析出 $\beta\text{-Mg}_{17}\text{Al}_{12}$ 共晶物,此种共晶物熔点较低,加之由于熔核区域与母材区域不规则过度以及晶粒尺寸过度较快引起的应力集中,此区域在凝固结晶后期,容易出现裂纹,将形成点焊接头脆性破坏和断裂的发源地^[5].镁合金侧接头熔核组织主要由柱状晶和等轴晶组成.在结晶前沿液体中有适当的过冷度,这一过冷度很小,使之不能形成新的晶核,只能靠晶粒的继续长大来进行.晶体沿其相反的方向择优长成柱状晶,其中以垂直于电极表面方向长大速度最快,迅速的优先长入液体中.而与散热方向倾斜的枝晶束受到彼此限制不能侧向生长,只能沿散热方向生长,同时枝晶间的间距也不断地相互调整着,然后便形成了柱状晶(图6b).镁合金导热性好,降温速度极快,使得在熔核的中心液相中的温度梯度很小,形成成分过冷,结晶形核速率比长大速率更强烈地依赖于过冷度,再加上焊点在压力状态下结晶,进一步提高了均质形核率和异质形核率,使液态金属中形成大量的晶核,晶粒沿各个方向长大的速率差不多,就形成了等轴晶(图6c).镀锌钢侧热影响区微观组织由板条状马氏体、少量的铁

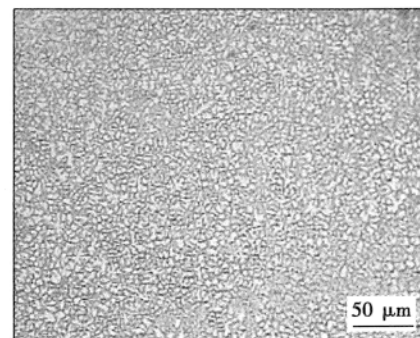
素体组成.形成机制为:钢的产热量远高于镁合金,镁合金自身和电极/钢的散热作用,最高温度出现在钢板的中心,从而促进了马氏体的转变,增加了马氏体的含量,冷却时形成了板条状马氏体(图6d).



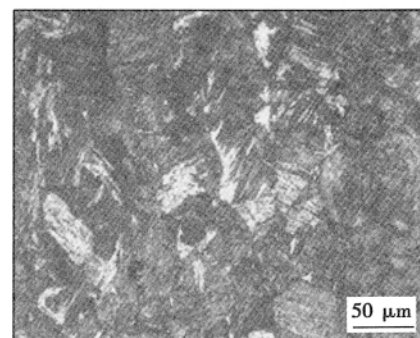
(a) 热影响区



(b) 柱状晶



(c) 等轴晶



(d) 铁素体和马氏体

图6 接头各区域显微组织

Fig. 6 Microstructure of weld joint region

2.3 接头的显微硬度分析

图 7 为在焊接时间为 8 周波,焊接电流为 32 kA,电极力为 8 kN 条件下,沿着焊缝中心的硬度分布。在镁合金侧,越靠近结合面硬度越高在结合面硬度最高,然而,在镀锌钢侧最高硬度出现在结合面和镀锌钢板的中心处。

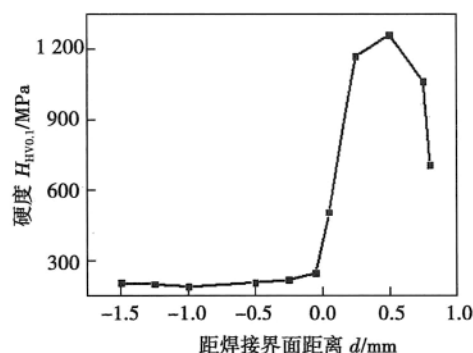


图 7 接头显微硬度

Fig. 7 Microhardness of joints

镁侧硬度的增加是由于合金强化的结果,在界面有更多的合金元素。而在钢侧由于钢的导电率远低于镁合金,钢侧的产热量远高于镁合金的产热量。所以钢可以作为一个热铁砧去加热镁合金,以及电极的散热导致热量的损失,所以最高温度出现在钢板的中心,从而促进了马氏体的转变,增加了马氏体的含量,最终导致了该位置的高硬度。

3 结 论

(1) 接头拉剪力随焊接工艺参数呈规律变化,在焊接时间 8 周波,焊接电流 32 kA,电极力 7 kN 时,达到最佳,接头强度达到 7 kN。

(2) 形成的接头由半椭圆形镁合金熔核和钢侧热影响区组成,镁合金侧熔核显微组织主要由柱状

晶和等轴晶组成,钢侧热影响区显微组织为板条状马氏体。

(3) 镁侧母材硬度约(HV)为 202 MPa,镁侧熔核区的显微硬度(HV)约 215 MPa,在镀锌钢侧母材硬度(HV)在 740 MPa 左右,最高硬度出现在镀锌钢板中心约为 1 350 MPa。

参考文献:

- [1] 张伟华,孙大千,李志东,等. 电极板辅助点焊钢/铝异质接头的组织与性能[J]. 焊接学报,2011,32(9): 85-88.
Zhang Weihua, Sun Daqian, Li Zhidong, et al. Microstructure and mechanical property of dissimilar material resistant spot welded joint of steel and aluminum alloy with electrode plate[J]. Transactions of the China Welding Institution, 2011, 32(9): 85-88.
- [2] 余 琨,黎文献,王日初. 变形镁合金的研究、开发及应用[J]. 中国有色金属学报,2003,13(2): 277-288.
Yu Kun, Li Wenxian, Wang Richu. Research, development and application of wrought magnesium alloys[J]. The Chinese Journal of Nonferrous Metals, 2003, 13(2): 277-287.
- [3] 张高会,张平则,潘俊德. 镁及镁合金的研究现状与进展[J]. 世界科技研究与发展,2003,25(1): 72-78.
Zhang Gaohui, Zhang Pingze, Pan Junde. Research and developments of magnesium and magnesium alloys[J]. Scientific and Technological Research and Development In the World, 2003, 25(1): 72-78.
- [4] 郎 波,孙大千,任振安,等. 镁合金电阻点焊接头组织结构特点[J]. 焊接学报,2009,30(10): 33-36.
Lang Bo, Sun Daqian, Ren Zhennan, et al. Microstructure of magnesium alloy joints in resistant spot welding[J]. Transactions of the China Welding Institution, 2009, 30(10): 33-36.
- [5] 王亚荣,张忠典. 镁合金电阻点焊接头中的缺陷[J]. 焊接学报,2006,27(7): 9-12.
Wang Yarong, Zhang Zhongdian. Defects in joints for resistant spot welding of magnesium alloy[J]. Transactions of the China Welding Institution, 2006, 27(7): 9-12.

作者简介: 陈益平,男,1962 年出生,教授。主要从事电阻焊智能控制和集成制造等研究工作。Email: niatwi@163.com

116024 , China; 2. State Key Laboratory of Structural Analysis for Industrial Equipment , School of Aeronautics and Astronautics , Dalian University of Technology , Dalian 116024 , China) . pp 93 – 95 , 108

Abstract: The temperature field and residual stress field in the Invar steel film of LNG ship tank was numerically simulated using finite element software MSC. Marc , and the calculation of fatigue life of the welded joint was carried out with the welding residual stress field coupled with the liquid sloshing pressure. The calculated results show that the longitudinal residual stress in the centerline on weld surface was about 298 MPa , and the peak value of longitudinal residual stress reached 328 MPa , higher than the yield strength (280 MPa) of the Invar steel at room temperature. Because of the existence of the welding residual stress , the fatigue life of Invar steel welded joint decreased from about 2.1×10^6 to 1.7×10^5 .

Key words: Invar steel; welding residual stress; sloshing; fatigue life

3D finite element analysis of thermo-mechanical coupled field in solidification process during thermal spraying

LIU Guangjun , GENG Guihong (School of Materials Science and Engineering , Beifang University of Nationalities , Yinchuan 750021 , China) . pp 96 – 100

Abstract: With proper simplifications and assumptions , 3D finite element model of thermal-mechanical field was developed based on ANSYS software to numerically simulate distribution of temperature and stress fields upon solidification after thermally spraying nickel on steel substrate. The evolution of temperature and stress with time at some important spots in the coating was obtained and the effect of coating thickness on the stress in the interface between the coating and substrate was analyzed. The results show that the temperature in the coating gradually decreased from the center to the border. The residual stress on the coating was compressive , and increased with the increase of coating thickness.

Key words: thermal spraying; residual stress; numerical simulation; coupled field; finite element method

Analysis of microstructure and mechanical properties of dissimilar metal spot welded joint between magnesium alloy and steel

CHEN Yiping , SHAO Jinghui , HU Dean , CHENG Donghai (School of Aeronautic and Mechanical Engineering , Nanchang Hangkong University , Nanchang 330063 , China) . pp 101 – 104

Abstract: Three-phase secondary rectification spot welding machine was used to conduct dissimilar metal joining of magnesium alloy to steel , and the window of welding parameters and optimum parameters were obtained. The microstructure of the joints was examined with optical microscope and the microhardness in different zones was measured. The results show that the shearing strength increased initially and then decreased with the increase of welding time T (2 – 14 cycle) , welding current I

(20 – 37.5 kA) and electrode pressure P (5 – 8 kN) . The maximum shearing strength reached 6.961 kN when T was 8 cycle , I was 32 kA , and P was 7 kN. The joint was composed of nugget on magnesium alloy side , with equiaxed grains and columnar grains , and heat-affected zone on steel side , with lath martensite. On magnesium side , the closer distance of measured point to the fusion line , the higher the hardness was. The highest hardness appeared in the center of steel sheet on steel side.

Key words: dissimilar metal; resistance spot welding; processing parameters; microstructure

Effect of TIG-dressing on fatigue properties of 7N01 aluminum alloy welded joint

YAN Zhongjie¹ , LIU Xuesong¹ , FANG Hongyuan¹ , WANG Ping¹ , WANG Ren² , MENG Lichun² (1. State Key Laboratory of Advanced Welding and Joining , Harbin Institute of Technology , Harbin 150001 , China; 2. CSR Sifang Locomotive and Rolling Stock Co. , Ltd , Qingdao 266111 , China) . pp 105 – 108

Abstract: TIG-dressing of 7N01 aluminium alloy welded joint was carried out by shielded metal arc welding. The fatigue properties and microhardness of specimens were tested before and after TIG-dressing , and the fractography was analyzed with SEM and the composition in defect zone was examined with XRD. Experimental results show that TIG-dressing slightly reduced the stress concentration on the weld toe , however , TIG-dressing could also bring additional weld defects which would initiate fatigue crack. The reheating by TIG-dressing could soften the welded joint and degrade the resistance to fatigue crack propagation. Consequently , the fatigue life of welded joint after TIG-dressing slightly decreased. Therefore , it had no feasibility to improve the fatigue properties of 7N01 high strength aluminium alloy welded joint by TIG-dressing.

Key words: TIG-dressing; fatigue; welded joint

Semiconductor laser transmission welding of thermoplastic polypropylene

GONG Fei , HU Xiyuan , TAN Yun , WANG Chunming (School of Materials Science and Engineering , Huazhong University of Science and Technology , Wuhan 430074 , China) . pp 109 – 112

Abstract: With the development requirements of product lightweight , laser transmission welding of plastics is becoming a research focus , since it has good welding quality , controllability and is able to weld tiny parts. This paper discussed the effects of welding process factors , such as laser power , welding speed , clamping force and absorbent , on laser transmission welding of PP , using an 808 nm semiconductor laser. The shear strength of the joint was tested and the microstructure was examined after welding. The experimental results show that there was a proper range for welding heat input to obtain good weld formation and joint strength while keeping the clamping force and laser spot size constant.

Key words: laser transmission welding; thermoplastic; heat input; clamping force; absorbent